

Temperature effects on brittle fracture in cracked asphalt concretes

Majid-Reza Ayatollahi* and Sadjad Pirmohammad

*Fatigue and Fracture Laboratory, Center of Excellence in Experimental Solid Mechanics and Dynamics,
School of Mechanical Engineering, Iran University of Science and Technology,
Narmak, Tehran, 16846, Iran*

(Received February 26, 2012, Revised October 30, 2012, Accepted November 30, 2012)

Abstract. Cracking at low temperatures is one of the frequently observed modes of failure in asphalt concretes. In this investigation, fracture tests were performed on cracked asphalt concrete subjected to pure mode I and pure mode II loading at different subzero temperatures. An improved semi-circular bend (SCB) specimen containing a vertical crack was used to conduct the experiments. The SCB specimens produced from the gyratory compacted cylindrical samples were compressively loaded, and critical stress intensity factors, K_{Ic} and K_{IIc} , were then calculated using peak loads obtained from the tests. The experimental results showed that with decreasing the temperature, mode I and mode II critical stress intensity factors increased first but below a certain temperature they both decreased. It was also found that at a fixed temperature, the mode II fracture resistance of the asphalt concrete was higher than its mode I fracture resistance.

Keywords: asphalt concrete; fracture test; low temperature; mode I; mode II; brittle fracture

1. Introduction

Experimental observations have shown that asphalt concretes may experience various types of deteriorations such as cracking, rutting, shoving, etc. Such distresses not only decrease the pavement life and the road safety but also increase the maintenance and rehabilitation costs of roads and highways. This has prompted many researchers to improve the performance of asphalt concretes in order to improve their resistance against pavement deterioration (see for example Casey *et al.* 2008, Al-Hadidy and Yi-qiu 2009, Chen *et al.* 2009, Ahmadiania *et al.* 2011).

Thermal cracking is one of the major modes of failure in asphalt pavements particularly in the cold regions. The extension of the cracks generated by thermal cracking is then accelerated by traffic loads. Cold climate causes asphaltic materials to lose their ductility and to fail in a brittle manner at subzero temperatures. Similar behavior has also been reported for some other materials like polymethyl-methacrylate (PMMA) at low temperatures (Gómez *et al.* 2008a). Numerous researchers have employed linear elastic fracture mechanics (LEFM) to study fracture behavior of asphalt concretes at low temperatures (see for example Dongre *et al.* 1989, Marasteanu *et al.* 2002,

*Corresponding author, Professor, E-mail: m.ayat@iust.ac.ir

Tekalur *et al.* 2008).

Reflective cracking is another prevalent asphalt concrete distress that takes place almost in all types of asphalt pavements. Movements at the crack tip resulting from mechanical and environmental loads cause a reflective crack to develop upward. Development mechanism of reflective cracks within the road pavement is attributed to three types of deformation: bending, shear and thermal (see Fig. 1). However, in practice often a combination of them takes place. Shear deformation affects the mechanism of crack growth significantly not only for reflective cracks but also for top-down cracks, particularly when a vehicle approaches or moves away from the crack plane. For example, Ameri *et al.* (2011) have recently shown that the shear type of deformation plays an important role in the top-down crack propagation.

Mode I fracture in hot mix asphalt (HMA) mixtures has been examined by many researchers in the recent decades. For instance, Kim and Hussein (1997) measured the mode I fracture toughness of HMA at temperatures ranging from -5°C to -30°C . In addition, Molenaar and Molenaar (2000) employed the semi-circular bend (SCB) specimens to find the mode I critical stress intensity factor, K_{Ic} , for different types of asphalt mixtures. In another investigation, Li *et al.* (2004) studied the cracking behavior of asphalt concretes using the SCB specimen. They examined three types of asphalt mixtures at different temperatures and obtained their fracture properties including fracture toughness. Moreover, Wagoner *et al.* (2005) measured the fracture toughness of an asphalt concrete using disc shaped compact tension (DC-T) test. Meanwhile, very few investigations have dealt with mode II fracture in asphalt pavements. Artamendi and Al-Khalid (2006) used LEFM to investigate the asphalt concrete behavior under mixed mode I-II loading but only at one temperature. The important role of shear deformation in the final deterioration of top-down and reflective cracks, as mentioned earlier, underlines the requirement for more detailed investigations on mode II (or shear) fracture in asphalt mixtures.

Mode II and mixed mode I/II brittle fracture occur in many engineering applications. This has prompted numerous investigators to propose failure criteria suitable for predicting the onset of fracture in such applications. A list of some relevant criteria can be seen below for cracked or notched components. Further details can be found in the references given for each criterion.

- *Maximum tangential stress (MTS):*
Erdogan and Sih (1963) for cracked components and (Ayatollahi and Torabi 2010) for notched components.
- *Generalized maximum tangential stress (GMTS):*
Smith *et al.* (2001), Ayatollahi *et al.* (2006), Ayatollahi and Aliha (2009)
- *Maximum energy release rate (G):*
Hussain *et al.* (1974)
- *Strain energy density (SED):*
Sih (1974), Lazzarin and Berto (2005), Lazzarin *et al.* (2006), Gómez *et al.* (2007, 2009)
- *Cohesive zone model (CZM):*
Hillerborg *et al.* (1976), Elices *et al.* (2002), Elices *et al.* (2008).
- *Generalized notch stress intensity factor:*
Gómez *et al.* (2008^b), Atzori *et al.* (2005)
- *Fictitious notch rounding approach:*
Berto *et al.* (2008, 2012)

In the present investigation, numerous fracture tests were carried out under pure mode I and pure mode II loading at four different temperatures. The semi-circular bend (SCB) specimen together with a conventional three-point bend fixture were used to conduct the experiments. The SCB specimens were obtained from cylindrical samples prepared by Superpave Gyratory Compactor (SGC), and an artificial crack was generated within the SCB specimen using a very thin blade. The mode I and mode II critical stress intensity factors were eventually calculated utilizing the peak loads measured from the fracture tests.

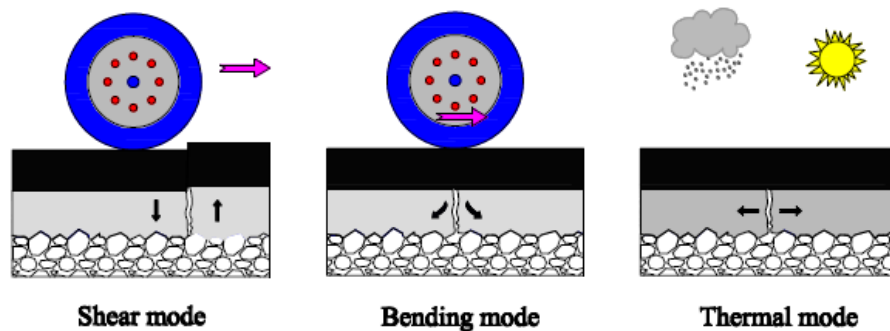


Fig. 1 Different states of deformation in a reflective crack under traffic loads and environmental effects

2. Test specimen

A cracked body may experience three different types of loading, in terms of crack face displacements i.e., mode I, mode II, and mode III standing for opening, sliding, and tearing modes, respectively. Under complex loading conditions, often a combination of these three modes takes place. In a cracked asphalt concrete, as shown in Fig. 1, thermal strains generate opening deformation (mode I), and traffic loads cause both opening (mode I) and shear types of deformation (mode II or mode III). While mode III loading is rarely observed in HMA (Lytton 1989, Mukhtar and Dempsey 1996), mode I and mode II loading are the prevalent modes of failure in the asphalt pavements containing reflective cracks or top-down cracks.

Different types of test specimens such as the single edge notched beam (SENB), the semi-circular bend (SCB), the disk-shaped compact tension (DC-T) have been employed in the past by researchers to evaluate fracture behavior of engineering materials under mode I or mixed mode loading (see e.g., Ayatollahi and Aliha 2006, Ayatollahi *et al.* 2006, Ayatollahi and Aliha 2007). The SCB specimen is very suitable for fracture tests on asphalt mixtures because it can be easily prepared by using the Superpave Gyratory Compactor (SGC) or from the cores obtained directly from the pavement layer. Moreover, experiments under different modes of loading can be conveniently conducted via a simple three-point bend fixture. Therefore, in the present research, an improved semi-circular bend specimen shown schematically in Fig. 2 was employed to conduct experiments under pure mode I and pure mode II loading. A semi-circular specimen of radius $R = 75$ mm containing a vertical edge crack of length $a = 20$ mm emanating normal to the flat edge of the specimen is compressively loaded. Ayatollahi (2011) has recently performed extensive finite element analyses to study the modified SCB specimen under different combinations of mode I and

mode II. It is reminded that pure mode I and pure mode II loading occur when K_{II} and K_I , respectively, are zero in the cracked component. Ayatollahi (2011) varied the crack position (L) in the same SCB specimen by performing numerous finite element analyses, and finally found that pure mode II loading takes place when $L = 16$ mm, while for mode I loading L should be zero (i.e., the crack should be in the middle of specimen). In those FE analyses, parameters shown in Fig. 2 namely the radius R , the thickness t , the crack length a and the load P were assumed to be 75 mm, 32 mm, 20 mm and 1000 N, respectively. The distances of bottom supports from the center line (i.e., S_1 and S_2) were both 50 mm for pure mode I loading, and 50 mm and 20 mm, respectively, for pure mode II loading. Meanwhile, in the FE analyses, the Young's modulus E and Poisson's ratio ν were taken 12.5GPa and 0.35, according to Timm *et al.* (1998). The stress intensity factors K_I and K_{II} were obtained directly from the FE results as 194.79 kPa.m^{1/2} and 117.50 kPa.m^{1/2}, respectively. These parameters can be written in terms of the applied load P as:

For pure mode I

$$K_I = Y_I \left(\frac{a}{R}, L, S_1, S_2 \right) \frac{P}{2Rt} \sqrt{\pi a} \quad (1)$$

For pure mode II

$$K_{II} = Y_{II} \left(\frac{a}{R}, L, S_1, S_2 \right) \frac{P}{2Rt} \sqrt{\pi a} \quad (2)$$

where, Y_I and Y_{II} are dimensionless parameters called mode I and mode II geometry factors, respectively. By replacing the values of K_I , K_{II} , P , R , t and a into Eqs. (1) and (2), Y_I and Y_{II} were obtained as 3.73 and 2.25, respectively. These geometry factors Y_I and Y_{II} are utilized later for obtaining the mode I and mode II critical stress intensity factors, respectively.

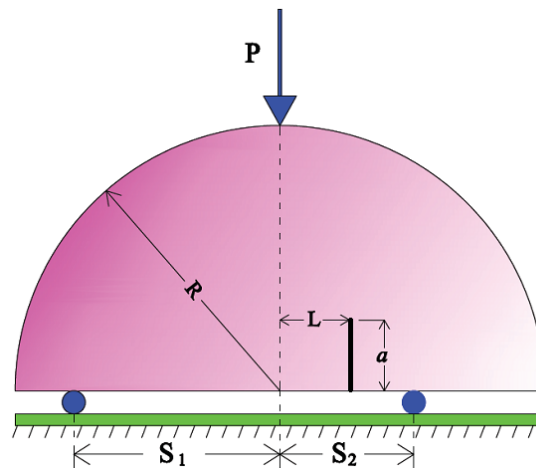


Fig. 2 The modified semi-circular bend (SCB) specimen

3. Experimental program

3.1 Material and specimen preparation

The HMA mixtures are composed of three main components including aggregates, binders and air voids. Aggregates are extracted from natural rocks and constitute about 95% by weight of HMA mixtures. They can be classified by their size which is determined by sieves with standard openings (e.g., 12.5 mm, 9.5 mm, 4.75 mm and so on). Aggregate gradation gives the percentage of each of the sizes in a HMA mixture. The size distribution of aggregate particles is directly related to the performance of the HMA mixtures. The aggregate gradation employed in the present paper is similar to the one known as aggregate gradation No. 4 (see Table 1), according to the Iran highway asphalt paving code, and is extensively used in the Iran highway networks. Binders which constitute about 5% by weight of HMA mixtures stick aggregates together, and are classified by a parameter called “penetration grade” stating softness of the binder. Binders with the penetration grades of 40-50, 60-70 and 85-100 are the common ones which are frequently used in the road pavements. A binder with penetration grade of 60–70, most widely used in the Iran pavement systems, was used in the preparation of the HMA mixture studied in the present research study. Moreover, the percent air void affects the density of HMA mixtures such that by increasing the air void, the HMA density decreases. The air void content of 4 percent was used for preparing the HMA mixtures.

In order to produce the SCB specimens, first cylindrical samples of diameter 150 mm and height 130 mm were compacted in the laboratory using the superpave gyratory compactor (SGC). The cylindrical samples were then sliced into three circular plates of 32 mm thickness by means of a water-cooled masonry saw (see Fig. 3(a)). Each plate was then cut from the center line to obtain two semi-circular specimens using another water-cooled sawing machine with a diamond tipped blade of 1 mm thickness (as shown in Fig. 3(b)). Therefore, six SCB specimens were acquired from each cylindrical sample. To create an artificial crack within the SCB specimen, a vertical edge crack of length 20 mm was generated using the sawing machine shown in Fig. 3(c) with a very thin blade (0.3 mm in thickness). Fig. 4 displays a typical crack generated within the SCB specimen.

Table 1 HMA aggregate gradation

Sieve size (mm)	Requirements		Percent passing
	Min	Max	
19	100	100	100
12.5	90	100	95
9	67	87	77
4.75	44	74	59
2.36	28	58	43
1.18	20	46	33
0.5	13	34	23
0.3	5	21	13
0.15	4	16	9.5
0.075	2	10	8.4

3.2 Fracture tests

Three-point bend fracture tests were conducted on the cracked SCB specimens under either pure mode I or pure mode II loading at several subzero temperatures of 0 °C, -10 °C, -20 °C, and -35 °C. Each SCB specimen was first put into a freezer with the fixed test temperature for 4 hours. Tests were then carried out immediately using a universal testing machine and a three-point bend fixture. All tests were performed with a constant displacement rate of 3 mm/min. The load-load line displacement curve was recorded for each fracture test. Fig. 5 shows two samples of the load-load line displacement curves recorded from the mode I and mode II fracture tests at -20 °C. It is seen that the load increases linearly and then suddenly drops to zero, confirming the predominantly linear elastic behavior of fractured specimens. Therefore, the concepts of LEFM can be considered to be applicable in analyzing the test results. Once the fracture load P_{cr} is obtained from the experiments the critical stress intensity factors K_{Iff} and K_{IIff} can be determined using

$$K_{Iff} = Y_I \frac{P_{Icr}}{2Rt} \sqrt{\pi a} \quad (3)$$

for pure mode I tests and

$$K_{IIff} = Y_{II} \frac{P_{IIcr}}{2Rt} \sqrt{\pi a} \quad (4)$$

for pure mode II tests.

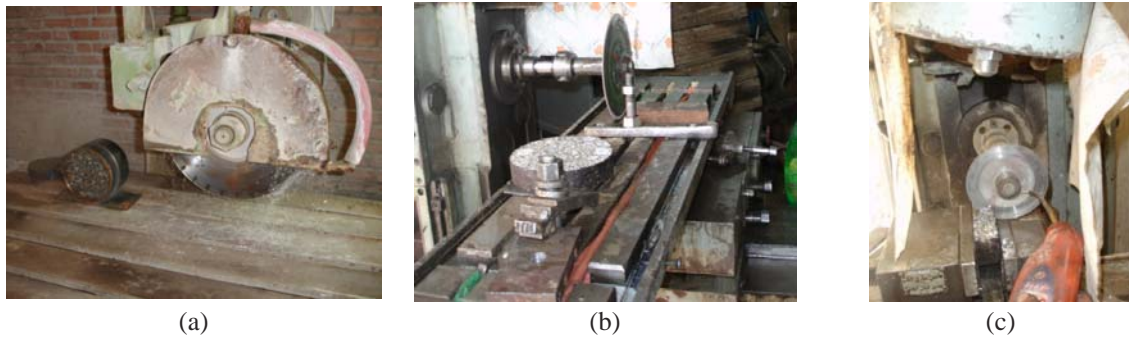


Fig. 3 (a) water-cooled masonry sawing machine for cutting the asphalt cylinder into discs, (b) water-cooled sawing machine for cutting each disc into two SCB specimens, (c) water-cooled sawing machine for generating crack in SCB specimen



Fig. 4 An asphalt SCB speimen containing a thin crack

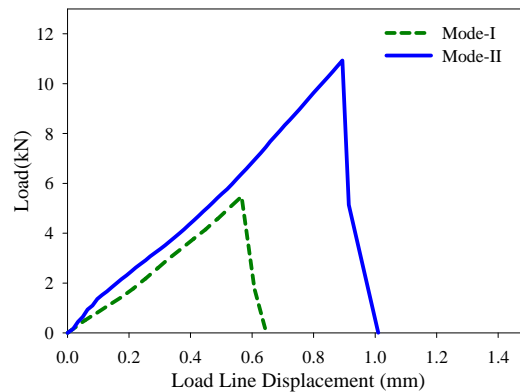


Fig. 5 Load versus load line displacement at -20°C

4. Results and discussion

Mode I fracture tests were conducted at different low temperatures as described earlier. Fig. 6(a) shows the test set-up for experiments performed under pure mode I loading. In order to increase the reliability of experimental results, four replicates were tested at each set of specimen temperature and mode of loading. Fracture loads P_{Icr} were recorded from the test machine and then the corresponding critical stress intensity factors K_{Ic} were calculated using Eq. (3). Table 2 presents the values of fracture load and K_{Ic} obtained from the mode I fracture experiments together with the average K_{Ic} for each specimen temperature.

Mode II fracture tests were carried out by locating the bottom supports in appropriate positions as described in section 2. The same conventional round-tip fixtures utilized for mode I tests were initially used for mode II experiments. However, some of the tests were not successful, because fracture initiated from the lower and right hand side bottom support instead of taking place from the crack tip (see Fig. 6(b)). This unfavorable point of failure initiation can be attributed to excessive stress concentration in the region where the load was applied to the specimen through the right support.



Fig. 6 Test configuration, (a) mode I fracture test, (b) unsuitable fixture setting for mode II fracture test

Table 2 Experimental results obtained from mode I fracture tests

Specimen temperature	Replicate No.	$P_{I_{cr}}$ (kN)	K_{I_f} (MPa \sqrt{m})	$K_{I_f}^{av}$ (MPa \sqrt{m})
0°C	1	4.507	0.8789	0.8162
	2	4.025	0.7849	
	3	4.245	0.8278	
	4	3.965	0.7732	
-10°C	1	4.836	0.9430	0.8961
	2	4.325	0.8434	
	3	4.764	0.9290	
	4	4.456	0.8689	
-20°C	1	5.121	0.9986	1.0376
	2	5.636	1.0990	
	3	5.476	1.0678	
	4	5.052	0.9851	
-35°C	1	4.595	0.8960	0.8240
	2	3.514	0.6852	
	3	3.919	0.7642	
	4	4.874	0.9504	

To avoid crack initiation from undesirable locations, the lower fixtures were modified such that instead of applying the bottom loads in concentrated points (as was the case in the mode I test set-up) the loads were applied as distributed forces. Several finite element analyses were performed to find the appropriate width of distributed load (i.e., the magnitude of b in Fig. 7(a)) in order to provide pure mode II loading. A pictorial representation of the modified test configuration has been displayed in Fig. 7(a). The appropriate value of parameter b was found to be 4 mm. Thus, the conventional fixtures used in the first set-up were replaced with the second one, and a new set of fracture tests were performed in which the crack initiation took place properly i.e., from the crack tip (see Fig. 7(b)). By this modification the stress concentration at bottom supports was reduced, and pure mode II fracture tests were successfully simulated experimentally using the SCB specimens. The load-load line displacement curve was recorded and the mode II critical stress intensity factor K_{II_f} was calculated by replacing the maximum load obtained from the test into Eq. (4). The results obtained from the mode II fracture tests have been presented in Table 3. Fig. 8 shows samples of the SCB specimens fractured under pure mode I and pure mode II loadings. It is seen that, for mode II fracture tests, the crack extension was initiated from the crack tip and propagated through the aggregates towards the upper fixture where the displacement-controlled load was applied. While, crack growth in mode I specimens was self-similar, the fracture initiation direction in mode II specimens made an angle with respect to the pre-existing crack. It is worth noting that because of the heterogeneity of the asphalt concretes, crack path in the broken asphalt concrete specimen is not smooth, and a slight zigzag pattern exists. This can be seen in Fig. 8. For the sake of comparison, the mean fracture loads for different temperatures and modes of loading have been shown in Fig. 9. The curves fitted to the experimental results show that the mode I and mode II fracture loads initially increase by reducing the specimen temperature but after reaching a peak value at a temperature around -20°C, they both decline. According to Fig. 9, the mode II fracture loads in the SCB specimens are more than twice the mode I fracture loads, suggesting that the fracture strength of asphalt concrete under shear loading is higher than its value under tensile

(opening) loading. Similar behavior (i.e., higher mode II fracture load compared with mode I fracture load) has been reported in some other experiments performed on brittle materials like polycrystalline graphite (Ayatollahi *et al.* 2011, Ayatollahi and Torabi 2011). On the other hand, the variation of fracture load against temperature for mode II loading is steeper than that of mode I loading; which indicates that a cracked asphalt concrete subjected to shear loads is more sensitive to the temperature than that subjected to tensile loads.

Table 3 Fracture results for mode II loading

Specimen temperature	Replicate No.	P_{IIcr} (kN)	K_{II} (MPa \sqrt{m})	K_{II}^{av} (MPa \sqrt{m})
0°C	1	7.975	0.9280	0.9261
	2	8.220	0.9565	
	3	7.966	0.9270	
	4	7.674	0.8930	
-10°C	1	9.955	1.1584	1.1113
	2	9.925	1.1550	
	3	8.842	1.0289	
	4	9.479	1.1031	
-20°C	1	11.779	1.3707	1.3025
	2	10.830	1.2603	
	3	10.930	1.2719	
	4	11.232	1.3071	
-35°C	1	7.845	0.9129	0.9645
	2	7.288	0.8481	
	3	8.732	1.0161	
	4	9.288	1.0808	

Fig. 10 shows the average values of the critical stress intensity factors (K_{I} and K_{II}) for four different temperatures. It is seen that for the experiments performed under mode I loading, by reducing the specimen temperature, K_{I} increases first but decreases when the temperature drops below a certain value. Similar observations on mode I fracture resistance of asphalt concretes have been reported in other papers like Kim *et al.* (2003), and Kim and Hussein (1997) as well. The accelerated road deteriorations in the cold regions can be due to the decrease in the crack growth resistance of the HMA mixtures at lower temperatures (below -20°C). Indeed, when the temperature is reduced, the strength of asphalt cement increases. This can be the main reason for the initial increase of the mode I fracture load and its corresponding critical stress intensity factor. Furthermore, reduction of the mode I critical stress intensity factor below a certain temperature can be attributed to the internal damage caused by the differential thermal contraction (DTC) between the binder and the aggregate. More details on the DTC damage mechanism can be found in papers like Hussein and Halim (1993), and Kim and Hussein (1995). Fig. 10 also reveals that the trend of the variations of the K_{II} against temperature is similar to the trend for K_{I} . Again, the initial enhancement of K_{II} can be linked to the property of binder (i.e. the temperature reduction leads to an increase in the binder strength) and the following decrease of K_{II} can be related to the DTC damage. Moreover, Fig. 10 shows that the mode II critical stress intensity factor is higher than mode I critical stress intensity factor. In other words, asphalt concretes exhibit better resistance

against brittle fracture under shear loads than under tensile loads. Enhanced fracture resistance under shear loads has been seen in some other experimental studies conducted on glass (Ayatollahi and Aliha 2009), graphite (Awaji and Sato 1978) and dental resins (Ayatollahi and Aliha 2008). Fig. 11 displays the variations of K_{II}/K_{I} against temperature where a trend similar to those of K_{I} and K_{II} is observed.

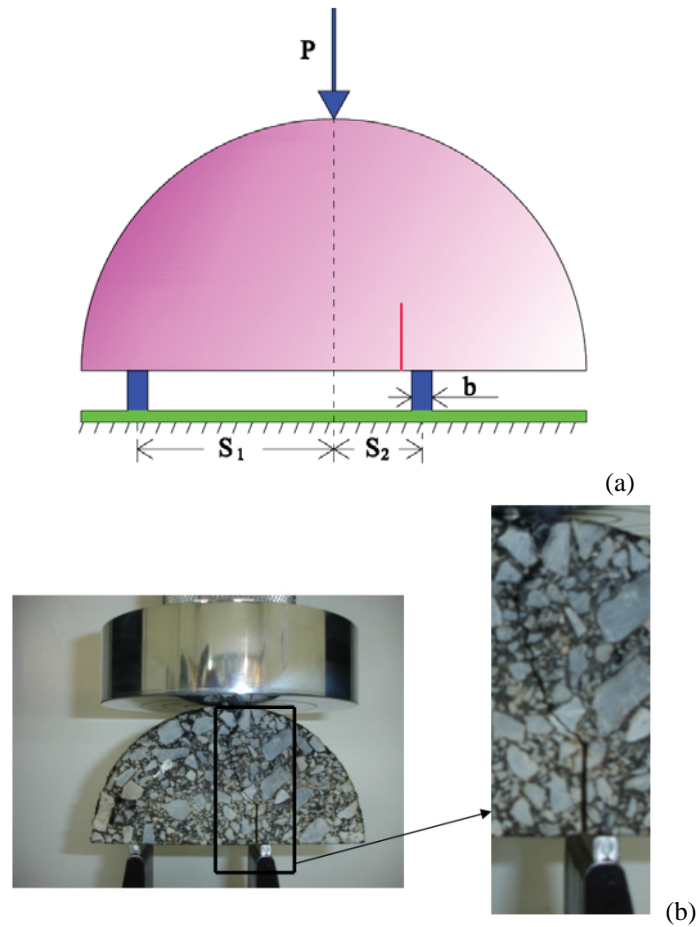


Fig. 7 (a) Three-point bend test (second test set-up), (b) fracture test using second set-up

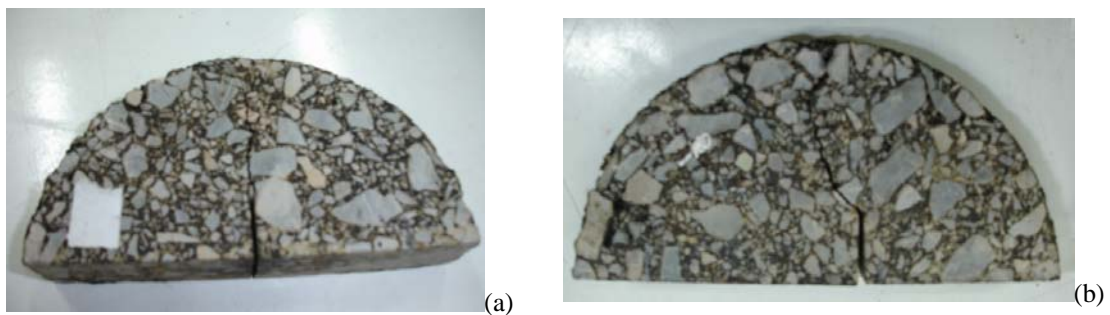


Fig. 8 Samples of SCB specimens after the fracture test, (a) mode I loading, (b) mode II loading

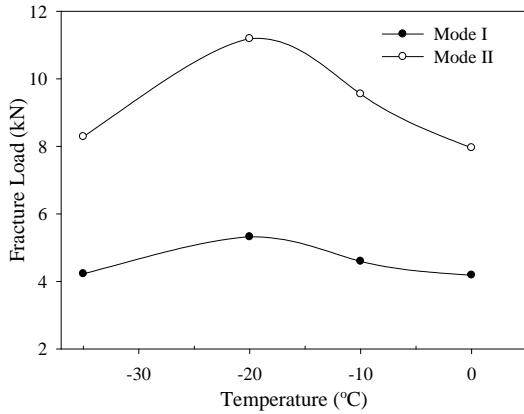


Fig. 9 Mode I and mode II fracture loads versus the specimen temperature

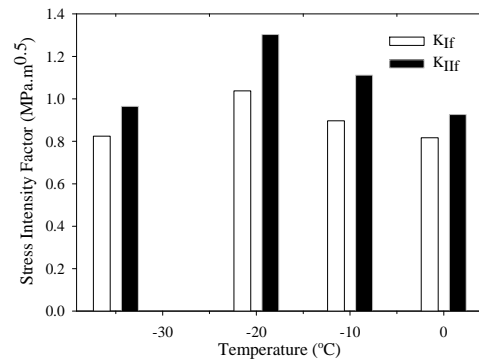


Fig. 10 Variations of critical stress intensity factors K_{I} and K_{II} versus temperature

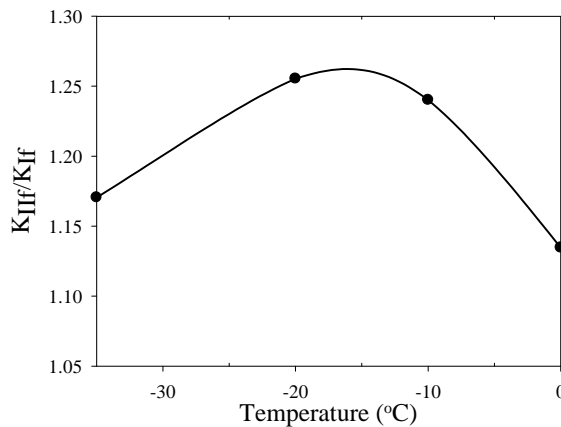


Fig. 11 Variations of the ratio of critical stress intensity factors K_{II}/K_{I} versus temperature

5. Conclusions

1. Pure mode I and pure mode II fracture tests were successfully performed on an asphalt concrete at several subzero temperatures using the semi-circular bend specimen.

2. The SCB specimen under pure mode II loading fractured at higher loads than under pure mode I loading. Furthermore, the slopes of the fracture load curves against temperature revealed that the fracture load in the cracked asphalt concrete subjected to shear loading was more sensitive to temperature than that subjected to tensile loading.

3. For the tested asphalt mixture, both mode I and mode II fracture loads initially increased by reducing the temperature, but for temperatures below -20°C , fracture loads dropped considerably.

4. The mode II critical stress intensity factor K_{II} at each temperature was higher than the mode I critical stress intensity factor K_{I} suggesting that cracked asphalt concrete resists against the shear

loads better than against the tensile loads.

5- For the SCB specimens tested under pure mode I loading, the fracture path was straight and along the direction of initial crack, whereas for the tests performed under pure mode II loading, the fracture trajectory was curvilinear, initiated from the crack tip with a certain angle relative to the pre-existing crack and extended towards the upper fixture.

References

- Ahmadinia, E., Zargar, M., Karim, M.R., Abdelaziz, M. and Shafiq, P. (2011), "Using waste plastic bottles as additive for stone mastic asphalt", *Mater. Des.*, **32**, 4844-4849.
- Al-Hadidy, A.I. and Yi-qiu, T. (2009), "Mechanistic approach for polypropylene-modified flexible pavements", *Mater. Des.*, **30**, 1133-1140.
- Ameri, M., Mansourian, A., Khavas, M.H., Aliha, M.R.M. and Ayatollahi, M.R. (2011), "Cracked asphalt pavement under traffic loading - A 3D finite element analysis", *Eng. Fract. Mech.*, **78**, 1817-1826.
- Artamendi, I. and Al-Khalid, H. (2006), "A comparison between beam and semi-circular bending fracture tests for asphalt", *Road Mater. Pavement Des.*, **6**, 163-180.
- Atzori, B., Filippi, S., Lazzarin, P. and Berto, F. (2005), "Stress distributions in notched structural components under pure bending and combined traction and bending", *Fatigue Fract. Eng. Mater. Struct.*, **28**, 13-23.
- Awaji, H. and Sato, S. (1978), "Combined mode fracture toughness measurement by the disc test", *J. Eng. Mater. Tech.*, **100**, 172-175.
- Ayatollahi, M.R. (2011), Investigation of mixed mode fracture in asphalt concretes due to the traffic loads, Research Report 88B5T2P28(RP), Transportation Research Institute, Iran Ministry of Roads and Transportation.
- Ayatollahi, M.R. and Aliha, M.R.M. (2006), "On determination of mode II fracture toughness using semi-circular bend specimen", *Int. J. Solids Struct.*, **43**, 5217-5227.
- Ayatollahi, M.R. and Aliha, M.R.M. (2007), "Wide range data for crack tip parameters in two disc-type specimens under mixed mode loading", *Comput. Mater. Sci.*, **38**, 660-670.
- Ayatollahi, M.R. and Aliha, M.R.M. (2008), "On mixed-mode I/II crack growth in dental resin materials", *Scr. Mater.*, **59**, 258-261.
- Ayatollahi, M.R. and Aliha, M.R.M. (2009), "Mixed mode fracture in soda lime glass analyzed by using the generalized MTS criterion", *Int. J. Solids Struct.*, **46**, 311-321.
- Ayatollahi, M.R., Aliha, M.R.M. and Hassani, M.M. (2006), "Mixed mode brittle fracture in PMMA—An experimental study using SCB specimens", *Mater. Sci. Eng., A.*, **417**, 346-348.
- Ayatollahi, M.R., Berto, F. and Lazzarin, P. (2011), "Mixed mode brittle fracture of sharp and blunt V-notches in polycrystalline graphite", *Carbon*, **49**, 2465-2474.
- Ayatollahi, M.R. and Torabi, A.R. (2010), "Tensile fracture in notched polycrystalline graphite specimens", *Carbon*, **48**, 2255-2265.
- Ayatollahi, M.R. and Torabi, A.R. (2011), "Failure assessment of notched polycrystalline graphite under tensile-shear loading", *Mater. Sci. Eng., A.*, **528**, 5685-5695.
- Berto, F., Lazzarin, P. and Radaj, D. (2008), "Fictitious notch rounding concept applied to sharp V-notches: Evaluation of the micro structural support factor for different failure hypotheses. Part I: Basic stress equations", *Eng. Fract. Mech.*, **75**, 3060-3072.
- Berto, F., Lazzarin, P. and Radaj, D. (2012), "Fictitious notch rounding concept applied to V-notches with root holes subjected to in-plane shear loading", *Eng. Fract. Mech.*, **79**, 281-294.
- Casey, D., McNally, C., Gibney, A. and Gilchrist, M.D. (2008), "Development of a recycled polymer modified binder for use in stone mastic asphalt", *J. Resour. Conserv. Recy.*, **52**, 1167-1174.
- Chen, H., Xu, Q., Chen, S. and Zhang, Z. (2009), "Evaluation and design of fiber-reinforced asphalt mixtures", *Mater Des.*, **30**, 2595-2603.

- Dongre, R., Sharma, M.C. and Anderson, D.A. (1989), "Development of fracture criterion for asphalt mixes at low temperatures", *J. Transp. Res. Rec.*, **1228**, 94-105.
- Elices, M., Guinea, G.V., Gomez, F.J. and Planas, J. (2002), "The cohesive zone model: advantages, limitations and challenges", *Eng. Fract. Mech.*, **69**, 137-163.
- Elices, M., Rocco, C. and Roselló, C. (2008), "Cohesive crack modeling of a simple concrete: Experimental and numerical results", *Eng. Fract. Mech.*, **76**, 1398-1410.
- Erdogan, F. and Sih, G.C. (1963), "On the crack extension in plates under plane loading and transverse shear", *J. Basic Eng.*, **85**, 519-525.
- Gómez, F.J., Elices, M., Berto, F. and Lazzarin, P. (2007), "Local strain energy to assess the static failure of U-notches in plates under mixed mode loading", *Int. J. Fract.*, **145**, 29-45.
- Gómez, F.J., Elices, M., Berto, F. and Lazzarin, P.A. (2008a), "Fracture of U-notched specimens under mixed mode: Experimental results and numerical predictions", *Eng. Fract. Mech.*, **76**, 236-249.
- Gómez, F.J., Elices, M., Berto, F. and Lazzarin, P.A. (2008b), "A generalized notch stress intensity factor for U-notched components loaded under mixed mode", *Eng. Fract. Mech.*, **75**, 4819-4833.
- Gómez, F.J., Elices, M., Berto, F. and Lazzarin, P.A. (2009), "Fracture of V-notched specimens under mixed mode (I+II) loading in brittle materials", *Int. J. Fract.*, **159**, 121-135.
- Hillerborg, A., Modéer, M. and Petersson, P.E. (1976), "Analysis of crack formation and crack growth by means of fracture mechanics and finite elements", *J. Cement Concr. Res.*, **1**, 773-782.
- Hussain, M.A., Pu, S.L. and Underwood J. (1974) Strain energy release rate for a crack under combined mode I and mode II, Fracture analysis ASTM STP 560 American Society for Testing and Materials, Philadelphia, 2-28
- Hussein, H.M.E. and Halim, A.O.A. (1993), "Differential thermal expansion-contraction a mechanical approach to adhesion in asphalt concrete", *Can. J. Civ. Eng.*, **20**, 366-373.
- Kim, K.W. and Hussein, M. (1997), "Variation of fracture toughness of asphalt concrete under low temperatures", *J. Constr. Build. Mater.*, **11**, 403-411.
- Kim, K.W. and Hussein, M.E. (1995), "Effect of differential thermal contraction on fracture toughness of asphalt materials at low temperatures", *J. Assoc. Asphalt Paving Technol.*, **64**, 479-499.
- Kim, K.W., Kweon, S.J., Doh, Y.S. and Park, T.S. (2003), "Fracture toughness of polymer-modified asphalt concrete at low temperatures", *Can. J. Civ. Eng.*, **30**, 406-413.
- Lazzarin, P. and Berto, F. (2005), "From Neuber's elementary volume to Kitagawa and Atzori's diagrams: an interpretation based on local energy", *Int. J. Fract.*, **135**, 33-38.
- Lazzarin, P., Livieri, P., Berto, F. and Zappalorto, M. (2006), "Local strain energy density and fatigue strength of welded joints under uniaxial and multiaxial loading", *Eng. Fract. Mech.*, **75**, 1875-1889.
- Li, X., Marasteanu, M. and Assoc, J. (2004), "Evaluation of the low temperature fracture resistance of asphalt mixtures using the semi circular bend test", *J. Asphalt Paving Technol.*, **73**, 401-426.
- Lytton, R.L. (1989), "Use of geotextile for reinforcement and strain relief in asphalt concrete", *J. Geotextile Geomembranes*, **8**, 217-237.
- Marasteanu, M.O., Dai, S., Labuz, J.F. and Li, X. (2002), "Determining the low-temperature fracture toughness of asphalt mixtures", *J. Transp. Res. Rec.*, **1789**, 191-199.
- Molenaar, J.M.M. and Molenaar, A.A.A. (2000 of Conference), "Fracture toughness of asphalt in the semi-circular bend test", *2nd Eurasphalt and Eurobitume Congress*, Barcelona, Spain.
- Mukhtar, M.T. and Dempsey, B.J. (1996), Interlayer stress absorbing composite for mitigating reflective cracking in asphalt concrete overlays, UILU-ENG-96-2006, University of Illinois at Urbana-Champaign, Urbana, IL.
- Sih, G.C. (1974), "Strain-energy-density factor applied to mixed mode crack problems", *Int. J. Fract.*, **10**, 305-321.
- Smith, D.J., Ayatollahi, M.R. and Pavier, M.J. (2001), "The role of T-stress in brittle fracture for linear elastic materials under mixed mode loading", *Fatigue Fract. Eng. Mater. Struct.*, **24**, 137-150.
- Tekalur, S.A., Shukla, A., Sadd, M. and Lee, K.W. (2008), "Mechanical characterization of a bituminous mix under quasi-static and high-strain rate loading", *Constr. Build. Mater.*, **23**, 1795-1802.
- Timm, D., Birgisson, B. and Newcomb, D. (1998), "Development of mechanistic-empirical pavement design

- in Minnesota”, *J. Transp. Res. Rec.*, **1629**, 181-188.
- Wagoner, M.P., Buttlar, W.G., Paulino, G.H. and Blankenship, P. (2005), "Investigation of the fracture resistance of hot-mix asphalt concrete using a disk-shaped compact tension test", *J. Transp. Res. Rec.*, **1929**, 183-192.